PAPER

Analysis of Bifurcation Phenomena on Two Chaotic Circuits Coupled by an Inductor

Masahiro WADA[†], *Student Member*, **Yoshifumi NISHIO**[†], *and* **Akio USHIDA**[†], *Members*

SUMMARY In this paper, we investigate bifurcation phenomena observed from two autonomous three-dimensional chaotic circuits coupled by an inductor. Two types of synchronization modes are observed in this coupled system, i.e., in-phase synchronization and anti-phase synchronization. For the purpose of detailed analysis, we consider the case that the diodes in the subcircuits are assumed to operate as ideal switches. In this case Poincaré map is derived as a three-dimensional map, and Lyapunov exponents can be calculated by using exact solutions. Various bifurcation phenomena related with chaos synchronization are clarified. We confirm that various bifurcation phenomena are observed from circuit experiments.

key words: *chaos, synchronization of chaos, bifurcation, breakdown of chaos synchronization, hyperchaos*

1. Introduction

Many nonlinear dynamical systems in various fields have been confirmed to exhibit chaotic oscillations. Recently applications of chaos to engineering systems are expected such as chaos noise generators, control of chaos, synchronization of chaos, and so on. In those applications, we are especially interested in synchronization of chaos. As far as we know, synchronization of chaos in a simple circuit was first reported by Saito et al.[1]. Since Pecora et al.[2] clarified such phenomena, a large number of studies on synchronization of chaos have been reported. However, the study on bifurcation of chaos synchronization has been started only recently [3]–[7]. Therefore, there remain a large number of unsolved problems related with bifurcation of synchronization of chaos.

In this paper, we investigate bifurcation phenomena observed from two autonomous three-dimensional chaotic circuits coupled by an inductor. This subcircuit is a simple chaotic circuit proposed by Inaba et al.[8]. Two types of synchronization modes are observed in this coupled system; namely in-phase synchronization and anti-phase synchronization. Throughout this paper we use the word "chaos synchronization" as follows. Two continuous time chaotic signals $S_1(t)$ and $S_2(t)$ are said to be synchronized *completely* at in-phase, if $\lim_{t\to\infty} |S_1(t) - S_2(t)| = 0$ (or at anti-phase if $\lim_{t\to\infty} |S_1(t) + S_2(t)| = 0$). While two chaotic signals $S_1(t)$ and $S_2(t)$ are said to be synchronized *incompletely*, if $|S_1(t) \pm S_2(t)| < \varepsilon$, where the constant ε ($\neq 0$) is much smaller than the average amplitude of each chaotic signal. (The latter is not mathematical definition and is used only for qualitative explanation of the observed phenomena.) This system is a two subcircuit case of a coupled system in Ref[6]. However, in Ref[6], we did not analyze this circuit with the exact solutions in detail. Therefore, we will analyze various phenomena on this system in detail with the exact solution, especially paying attention to bifurcation route in each synchronization mode. For the purpose of detailed analysis, we consider the case that diodes in the subcircuits are assumed to operate as ideal switches. In this case the circuit equation in a piecewise linear region can be degenerated to a four-dimensional equation. Therefore, the associated Poincaré map is derived as three-dimensional map exactly using the analytical solutions. We can also calculate Lyapunov exponents from the Jacobian matrix obtained from the Poincaré map, This simplified technique was firstly reported by Inaba et al.[9] and was confirmed to be extremely effective in analyzing chaotic phenomena in dissipative electrical circuits. Further, this technique was extended to higher-dimensional circuits[10] and to circuits including two diodes[11]. However, it has not been applied for the analysis of chaos synchronization in coupled chaotic circuits. By calculating Lyapunov exponents, various bifurcation phenomena of chaos synchronization are clarified. Further, computer calculation results are confirmed by circuit experiments.

2. Circuit Model

The circuit model used in this study is shown in Fig. 1. In our system, two identical chaotic circuits which are simple chaotic subcircuits proposed by Inaba *et al.*[5] are coupled by an inductor L_0. This subcircuit is one of the simplest autonomous chaotic circuits consisting of only three memory elements, one linear negative resistor, and one diode.

At first, we approximate the characteristics of each diode by the following two-segment piecewise linear functions as in Fig. 2(a):

$$v_d(i_{L2k}) = \frac{r_d}{2}\left\{ i_{L2k} + \frac{V}{r_d} - \left| i_{L2k} - \frac{V}{r_d} \right| \right\} \qquad (1)$$

Manuscript received September 2, 1996.
Manuscript revised December 11, 1996.

[†]The authors are with the Faculty of Engineering, Tokushima University, Tokushima-shi, 770 Japan.

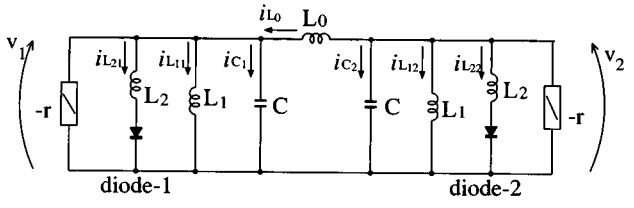

Fig. 1 Circuit model.

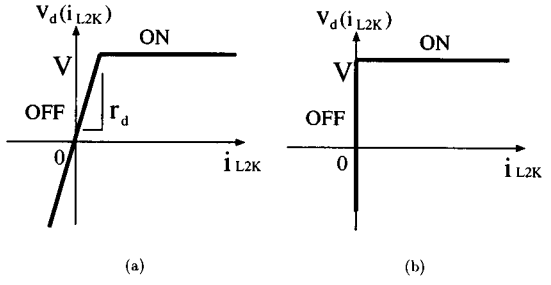

Fig. 2 Diode model.

where $k = 1, 2$. By changing the variables and parameters,

$$t = \sqrt{L_1 C}\,\tau, \quad \text{“}\cdot\text{”} = \frac{d}{d\tau}, \quad i_{L1k} = V\sqrt{\frac{C}{L_1}}x_k,$$

$$i_{L2k} = V\sqrt{\frac{C}{L_1}}y_k, \quad v_k = Vz_k.$$

$$\alpha = \frac{L_1}{L_0}, \ \beta = \frac{L_1}{L_2}, \ \gamma = \frac{1}{r}\sqrt{\frac{L_1}{C}}, \ \delta = r_d\sqrt{\frac{C}{L_1}}, \quad (2)$$

the normalized circuit equations are described by six-dimensional piecewise linear differential equations as follows:

$$\begin{aligned} \dot{x}_k &= z_k \\ \dot{y}_k &= \beta(z_k - f(y_k)) \\ \dot{z}_k &= (-1)^k\alpha(x_1 - x_2) - (x_k + y_k) + \gamma z_k \quad (3) \end{aligned}$$

$$f(y_k) = \frac{1}{2}\{\delta y_k + 1 - |\delta y_k - 1|\} \quad (4)$$

where $k = 1, 2$. The $f(y_k)$ is a piecewise linear function of y_k corresponding to the characteristic of the diode. We can calculate attractors by using the exact solution of Eq. (3). However, because it is hard to give rigorous representation of the Poincaré map and its Jacobian matrix, Lyapunov exponents cannot be calculated easily.

In order to calculate Lyapunov exponents by using exact solution, we consider the case that the diodes in the circuit are assumed to operate as ideal switches as shown in Fig. 2 (b). When this simplified model is used, the circuit equation is degenerated for the OFF state of the diodes. Because the current through the diode i_{L2k} is constrained to zero when the diode is OFF. Hence, when both diodes are OFF states, the circuit equation is degenerated to four-dimensional equation. It enables us to derive three-dimensional Poincaré map.

The circuit Eq. (3) is rewritten by using the diode model in Fig. 2 (b) as follows.

$$\begin{aligned} \dot{x}_k &= z_k \\ y_k &\cdots \begin{cases} y_k = 0 & \text{(OFF state)} \\ \dot{y}_k = \beta(z_k - 1) & \text{(ON state)} \end{cases} \\ \dot{z}_k &= (-1)^k\alpha(x_1 - x_2) - (x_k + y_k) + \gamma z_k \quad (5) \end{aligned}$$

where $k = 1, 2$. We define four piecewise linear regions as follows.

$\mathbf{D}_{11}$ ⋯ both diodes are ON states.
$\mathbf{D}_{10}$ ⋯ only right diode is OFF state.
$\mathbf{D}_{01}$ ⋯ only left diode is OFF state.
$\mathbf{D}_{00}$ ⋯ both diodes are OFF states.

The eigen-equation in each region is as follows.

$< \mathbf{D}_{11} >$:
$m^2\{m^4 - 2\gamma m^3 + 2(\alpha+\beta+1)m^2 - 2\gamma(\alpha+\beta+1)m + (2\alpha+\beta+1)(\beta+1)\} = 0$

$< \mathbf{D}_{10} >$:
$m\{m^4 - 2\gamma m^3 + (2\alpha+\beta+\gamma^2+2)m^2 - \gamma(2\alpha+\beta+2)m + (\alpha\beta+2\alpha+\beta+1)\} = 0$

$< \mathbf{D}_{01} >$:
$m\{m^4 - 2\gamma m^3 + (2\alpha+\beta+\gamma^2+2)m^2 - \gamma(2\alpha+\beta+2)m + (\alpha\beta+2\alpha+\beta+1)\} = 0$

$< \mathbf{D}_{00} >$:
$m^4 - 2\gamma m^3 + (2\alpha+\gamma^2+2)m^2 - 2\gamma(\alpha+1)m + (2\alpha+1) = 0$

The eigenvalues in each region are described as follows.

$\mathbf{D}_{11}$: ${}_{11}\sigma_1 \pm {}_{11}\omega_1$, ${}_{11}\sigma_2 \pm {}_{11}\omega_2$, 0, 0
$\mathbf{D}_{10}$: ${}_{10}\sigma_1 \pm {}_{10}\omega_1$, ${}_{10}\sigma_2 \pm {}_{10}\omega_2$, 0
$\mathbf{D}_{01}$: ${}_{01}\sigma_1 \pm {}_{01}\omega_1$, ${}_{01}\sigma_2 \pm {}_{01}\omega_2$, 0
$\mathbf{D}_{00}$: ${}_{00}\sigma_1 \pm {}_{00}\omega_1$, ${}_{00}\sigma_2 \pm {}_{00}\omega_2$

The exact solution in $\mathbf{D}_{01}$ derived from Eq. (5) is represented by using matrix as Eq. (6). $x_{10} \sim z_{20}$ are the initial conditions:

$$\begin{bmatrix} x_1(\tau) \\ z_1(\tau) - \frac{\alpha\beta}{\alpha\beta+2\alpha+\beta+1} \\ x_2(\tau) + \frac{\beta\gamma}{\alpha\beta+2\alpha+\beta+1} \\ y_2(\tau) - \frac{2\beta\gamma(1+\alpha)}{\alpha\beta+2\alpha+\beta+1} \\ z_2(\tau) - \frac{\beta(1+\alpha)}{\alpha\beta+2\alpha+\beta+1} \end{bmatrix}$$

$$= \mathbf{F}_{01}(\tau)\cdot\mathbf{F}_{01}^{-1}(0)\cdot\begin{bmatrix} x_{10} \\ z_{10} - \frac{\alpha\beta}{\alpha\beta+2\alpha+\beta+1} \\ x_{20} + \frac{\beta\gamma}{\alpha\beta+2\alpha+\beta+1} \\ y_{20} - \frac{2\beta\gamma(1+\alpha)}{\alpha\beta+2\alpha+\beta+1} \\ z_{20} - \frac{\beta(1+\alpha)}{\alpha\beta+2\alpha+\beta+1} \end{bmatrix} + \mathbf{A}_{01}\tau \quad (6)$$

where

$$\mathbf{F}_{01}(\tau) = [\mathbf{f}_1(\tau)\ \ \mathbf{f}_2(\tau)\ \ \mathbf{f}_3(\tau)\ \ \mathbf{f}_4(\tau)\ \ \mathbf{f}_5(\tau)]^T,$$

$$\mathbf{f}_2(\tau) = \begin{bmatrix} e^{{}_{01}\sigma_1\tau}\cos_{01}\omega_1\tau \\ e^{{}_{01}\sigma_1\tau}\sin_{01}\omega_1\tau \\ e^{{}_{01}\sigma_2\tau}\cos_{01}\omega_2\tau \\ e^{{}_{01}\sigma_2\tau}\sin_{01}\omega_2\tau \\ 0 \end{bmatrix}^T,$$

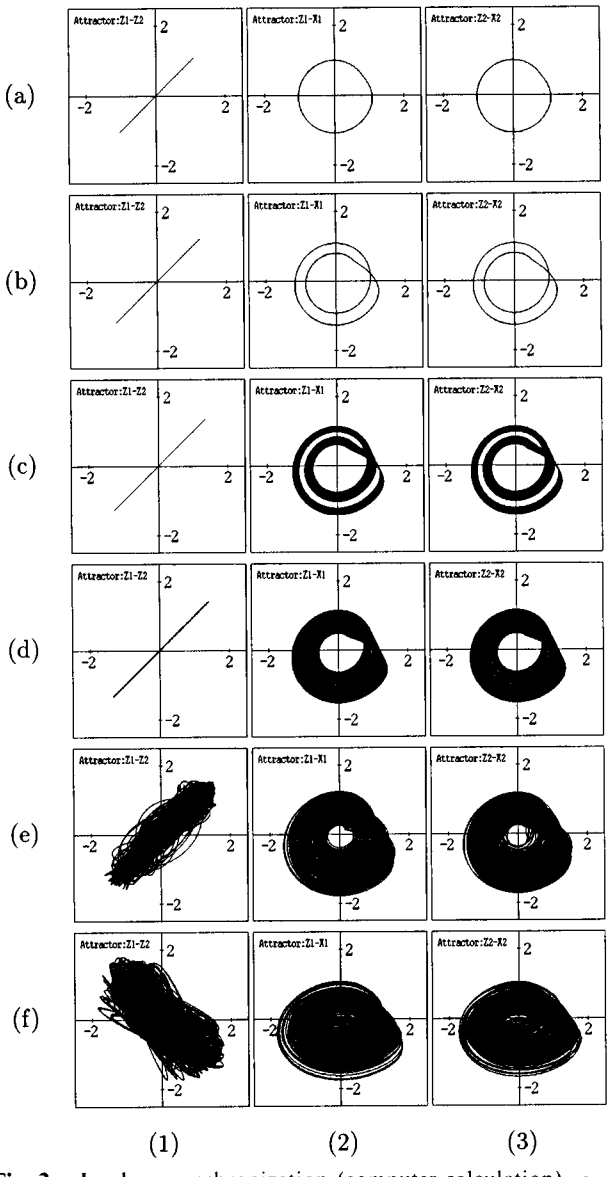

Fig. 3 In-phase synchronization (computer calculation). $\alpha = 0.60$, $\beta = 6.0$. γ : (a) 0.050, (b) 0.100, (c) 0.150, (d) 0.180, (e) 0.235, (f) 0.280. (1) z_1 vs. z_2. (2) z_1 vs. x_1. (3) z_2 vs. x_2.

$$\mathbf{f}_1(\tau) = \begin{bmatrix} \dfrac{\sigma_1 e^{01\sigma_1\tau}\cos_{01}\omega_1\tau}{\sigma_1^2+\omega_1^2} + \dfrac{\omega_1 e^{01\sigma_1\tau}\sin_{01}\omega_1\tau}{\sigma_1^2+\omega_1^2} \\ \dfrac{\sigma_1 e^{01\sigma_1\tau}\sin_{01}\omega_1\tau}{\sigma_1^2+\omega_1^2} - \dfrac{\omega_1 e^{01\sigma_1\tau}\cos_{01}\omega_1\tau}{\sigma_1^2+\omega_1^2} \\ \dfrac{\sigma_2 e^{01\sigma_2\tau}\cos_{01}\omega_2\tau}{\sigma_2^2+\omega_2^2} + \dfrac{\omega_2 e^{01\sigma_2\tau}\sin_{01}\omega_2\tau}{\sigma_2^2+\omega_2^2} \\ \dfrac{\sigma_2 e^{01\sigma_2\tau}\sin_{01}\omega_2\tau}{\sigma_2^2+\omega_2^2} - \dfrac{\omega_2 e^{01\sigma_2\tau}\cos_{01}\omega_2\tau}{\sigma_2^2+\omega_2^2} \\ 1 \end{bmatrix}^T,$$

$$\mathbf{f}_3(\tau) = \frac{1}{\alpha}\left\{\frac{d}{d\tau}\mathbf{f}_2(\tau) + (1+\alpha)\mathbf{f}_1(\tau) - \gamma\mathbf{f}_2(\tau)\right\},$$

$$\mathbf{f}_5(\tau) = \frac{d}{d\tau}\mathbf{f}_3(\tau),$$

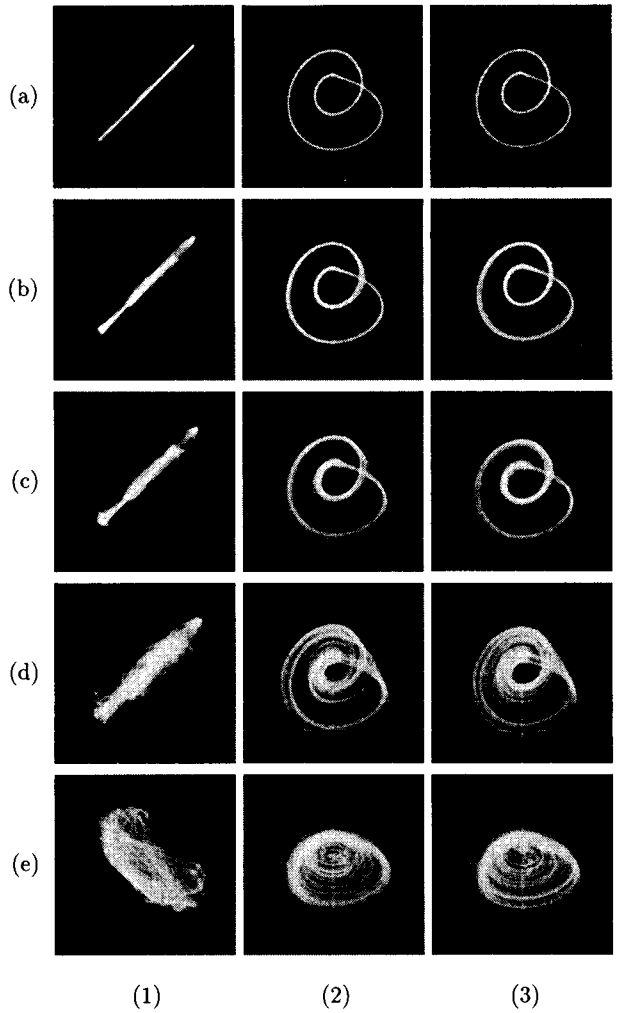

Fig. 4 In-phase synchronization (circuit experiment). $L_0 = 110.3\,\text{mH}$, $L_1 = 57.6\,\text{mH} \pm 0.1\%$, $L_2 = 10.2\,\text{mH} \pm 0.1\%$, $C = 68.3\,\text{nF} \pm 0.1\%$. (a) $r = 2.19\,\text{k}\Omega$, (b) $r = 2.15\,\text{k}\Omega$, (c) $r = 2.09\,\text{k}\Omega$, (d) $r = 1.87\,\text{k}\Omega$, (e) $r = 1.74\,\text{k}\Omega$. (1) $v_1$vs.v_2, Horizontal and Vertical: 0.5 V/div, (2) $v_1$vs.$i_{L_{11}}$, (3) $v_2$vs.$i_{L_{12}}$, Horizontal: 0.5 V/div, Vertical: 0.5 mA/div.

$$\mathbf{f}_4(\tau) = \alpha\mathbf{f}_1(\tau) - (\alpha+1)\mathbf{f}_3(\tau) + \gamma\mathbf{f}_5(\tau) - \frac{d}{d\tau}\mathbf{f}_5(\tau),$$

$$\mathbf{A}_{01} = \begin{bmatrix} \dfrac{\alpha\beta}{\alpha\beta+2\alpha+\beta+1} \\ 0 \\ \dfrac{\beta(1+\alpha)}{\alpha\beta+2\alpha+\beta+1} \\ -\dfrac{\beta(1+2\alpha)}{\alpha\beta+2\alpha+\beta+1} \\ 0 \end{bmatrix}.$$

We can similarly derive the exact solutions of other regions.

Figures 3 and 7 show chaotic attractors obtained by computer calculation. The two different synchronization modes coexist in this circuit and we can produce one of two modes by inputting a certain initial conditions. We will explain bifurcation phenomena of the two types of synchronizations in detail in later section.

3. Poincaré Map

In order to investigate the bifurcation route in detail, we consider the Poincaré map. We define the Poincaré section in the four-dimensional region $\mathbf{D}_{00}$ where both diodes are in the OFF state. In this case, the Poincaré map T can be derived as a three-dimensional map.

At first, we define the Poincaré section as

$$\mathbf{S}: \quad (y_1 = y_2 = 0, z_1 = 1, z_2 < 1) \cup (y_1 = y_2 = 0, z_1 < 1, z_2 = 1).$$

This Poincaré section corresponds to the transitional condition from the four-dimensional subspace D_{00} to D_{01} or D_{10}. Poincaré map T is represented by a composite map of some submaps which transform a point entering a subspace to a point exiting the subspace. Each submap can be represented by using the exact solution of Eq. (6). As an example, the submap T_Δ which transforms a point entering D_{01} from D_{00} to a point exiting to D_{11} is given by using the following equation. Then we defined that its route was Δ.

$$\begin{bmatrix} X_{11} - 0 \\ 1 - \frac{\alpha\beta}{\alpha\beta+2\alpha+\beta+1} \\ X_{21} + \frac{\beta\gamma}{\alpha\beta+2\alpha+\beta+1} \\ Y_{21} - \frac{2\beta\gamma(1+\alpha)}{\alpha\beta+2\alpha+\beta+1} \\ Z_{21} - \frac{\beta(1+\alpha)}{\alpha\beta+2\alpha+\beta+1} \end{bmatrix}$$

$$= \mathbf{F}_{01}(\tau_\Delta) \cdot \mathbf{F}_{01}^{-1}(0) \cdot \begin{bmatrix} X_{10} - 0 \\ Z_{10} - \frac{\alpha\beta}{\alpha\beta+2\alpha+\beta+1} \\ X_{20} + \frac{\beta\gamma}{\alpha\beta+2\alpha+\beta+1} \\ 0 - \frac{2\beta\gamma(1+\alpha)}{\alpha\beta+2\alpha+\beta+1} \\ 1 - \frac{\beta(1+\alpha)}{\alpha\beta+2\alpha+\beta+1} \end{bmatrix} + \mathbf{A}\tau_\Delta \tag{7}$$

where the initial point in D_{01} is $(x_1, y_1, z_1, x_2, y_2, z_2) = (X_{10}, 0, Z_{10}, X_{20}, 0, 1)$, the point on the transitional condition from D_{01} to D_{11} is $(X_{11}, 0, 1, X_{21}, Y_{21}, Z_{21})$ and τ_Δ is a transition time. Combination of submaps is determined by the route of the solution.

The Jacobian matrix DT of the Poincaré map T can be also derived rigorously as a product of some Jacobian matrices of the submaps. For example, Jacobian matrix of the submap T_Δ in Eq. (7) can be given as

$$DT_\Delta = \begin{bmatrix} 1 & -\frac{1}{-(1+\alpha)X_{11}+\alpha X_{21}+\gamma} & 0 & 0 & 0 \\ 0 & -\frac{Z_{21}}{-(1+\alpha)X_{11}+\alpha X_{21}+\gamma} & 1 & 0 & 0 \\ 0 & -\frac{\beta(Z_{21}-1)}{-(1+\alpha)X_{11}+\alpha X_{21}+\gamma} & 0 & 1 & 0 \\ 0 & -\frac{\alpha X_{11}-(1+\alpha)X_{21}-Y_{21}+\gamma Z_{21}}{-(1+\alpha)X_{11}+\alpha X_{21}+\gamma} & 0 & 0 & 1 \end{bmatrix}$$

$$\cdot \mathbf{F}_{01}(\tau_\Delta) \cdot \mathbf{F}_{01}^{-1}(0) \cdot \begin{bmatrix} 1 & 0 & 0 \\ 0 & 1 & 0 \\ 0 & 0 & 1 \\ 0 & 0 & 0 \\ 0 & 0 & 0 \end{bmatrix}. \tag{8}$$

4. In-Phase Synchronization

In this section, we investigate the in-phase synchronization. Computer calculated results and the corresponding circuit experimental results are shown in Figs. 3 and 4, respectively. Fig. 3 (a) shows in-phase synchronization of one-periodic attractors. As parameter γ increases, one-periodic attractor bifurcates to chaotic attractor via period-doubling route keeping in-phase synchronization. We can see that two circuits are synchronized completely at in-phase in spite of chaotic oscillations such as Fig. 3 (c). For these parameter values, the attractors are split to two bands by an unstable orbit. As γ increases, two bands of the chaotic attractor merges to one band and the attractor contains the unstable orbit. At the same time, chaos synchronization becomes incomplete as shown in Fig. 3 (d) (also see Fig. 5 (e)).POF5 It seems that the unstable orbit is deeply related to the breakdown of chaos synchronization. The detailed investigation of the influence is our important future research objective. As γ increases further, in-phase synchronization becomes unstable and only anti-phase synchronization is observed as in Fig. 3 (f).

The Poincaré map and its bifurcation diagram are shown in Figs. 5 and 6, respectively. We can verify the bifurcation route via period-doubling and breakdown of chaos synchronization.

Calculated Lyapunov exponents are shown in Fig. 7. We can see that the hyperchaos appears for the value of $\gamma \geqq 0.170$. It just corresponds to breakdown of in-phase synchronization of chaotic attractors. Namely, we can confirm for real circuit model that breakdown of chaos synchronization causes the generation of hyperchaos [4]. Further, we confirmed that for in-phase

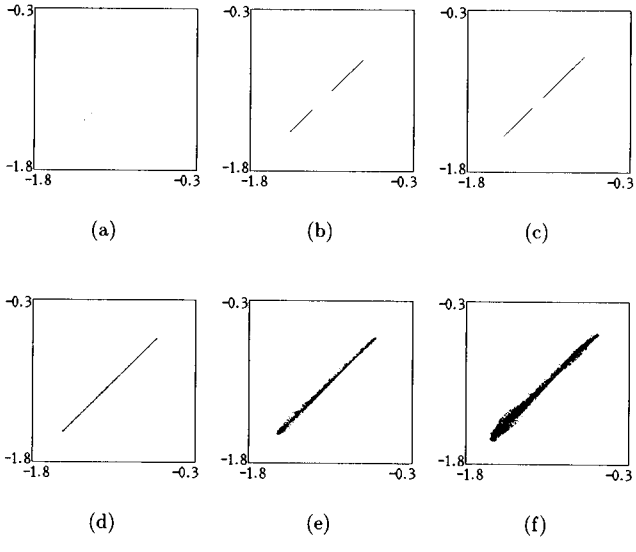

Fig. 5 Poincaré map of in-phase synchronization. Horizontal: x_1. Vertical: x_2. $\alpha = 0.60$. $\beta = 6.0$. γ : (a) 0.125, (b) 0.150, (c) 0.160, (d) 0.175, (e) 0.180, (f) 0.190.

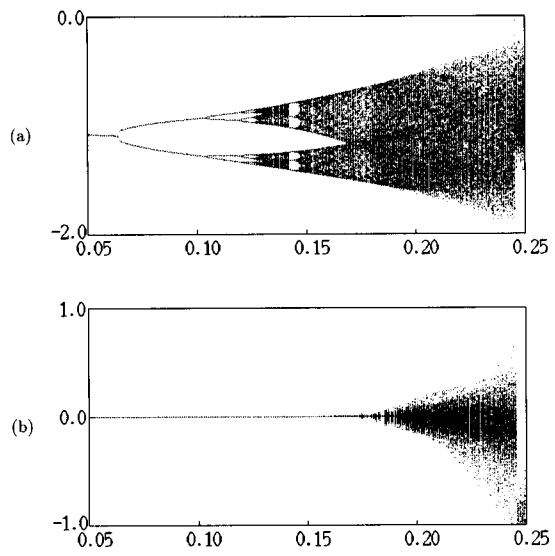

Fig. 6 Bifurcation diagram for the in-phase synchronization. $\alpha = 0.60$. $\beta = 6.0$. (a) Horizontal: γ, Vertical: x_1. (b) Horizontal: γ, Vertical: $x_1 - x_2$.

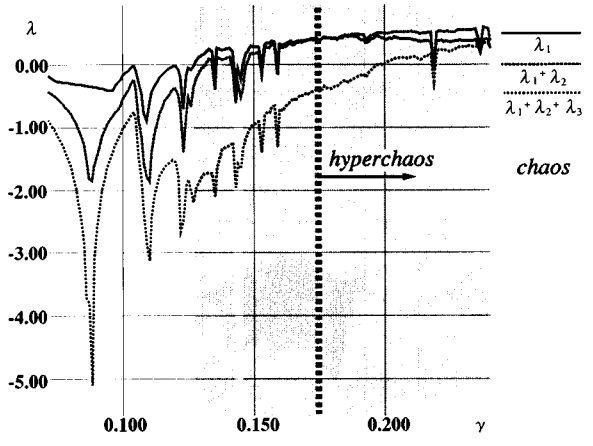

Fig. 7 Lyapunov exponents of the in-phase synchronization.

synchronization hyperchaos with 3 positive Lyapunov exponents does not appear.

5. Anti-Phase Synchronization

In this section, we investigate the anti-phase synchronization. Note that in-phase synchronizations and anti-phase synchronizations coexist in our circuit model. In the anti-phase synchronization mode, chaotic subcircuits cannot be synchronized completely, because the characteristics of the diode are not symmetric with respect to the origin.

Computer calculation results and the corresponding circuit experiments are shown in Figs. 8 and 9, respectively. We can see that one-periodic attractors of two circuits are synchronized at anti-phase completely as shown in Fig. 8 (a). However, we cannot see the complete synchronization for $\gamma > 0.08$. Because the

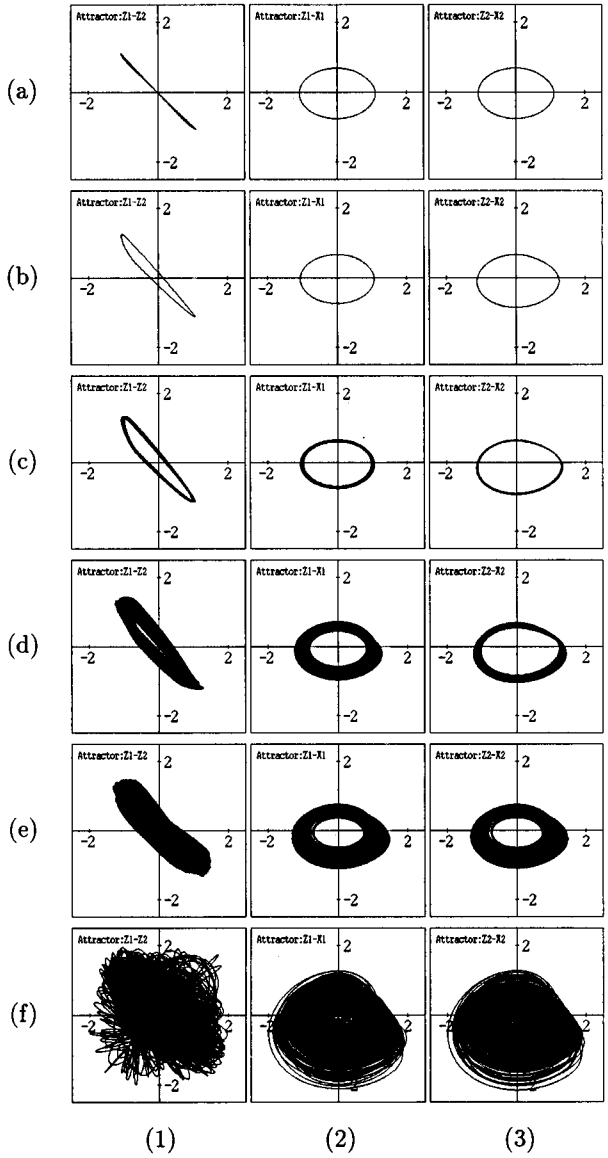

Fig. 8 Anti-phase synchronization (computer calculation). $\alpha = 0.60$, $\beta = 6.0$. γ : (a) 0.050, (b) 0.100, (c) 0.140, (d) 0.180, (e) 0.200, (f) 0.320. (1) z_1 vs. z_2. (2) z_1 vs. x_1. (3) z_2 vs. x_2.

attractor bifurcates to asymmetric one. The asymmetric one-periodic attractor (b) bifurcates to torus (c). As increasing parameter γ, the asymmetric chaotic attractor appears as shown in Fig. 8 (d). As γ is increased further, the symmetric chaotic attractor in Fig. 8 (e) appears. Finally, the anti-phase synchronization also becomes unstable and self-switching phenomenon of in-phase and anti-phase is observed as shown in Fig. 8 (f).

The Poincaré map and its bifurcation diagram are shown in Figs. 10 and 11, respectively. We can verify the bifurcation route via Hopf bifurcation. We can see that one-periodic attractor (a), bifurcates to torus (b), (c) and (d), and also observe torus breaks down and chaos appears (e).

Calculated results of Lyapunov exponents are

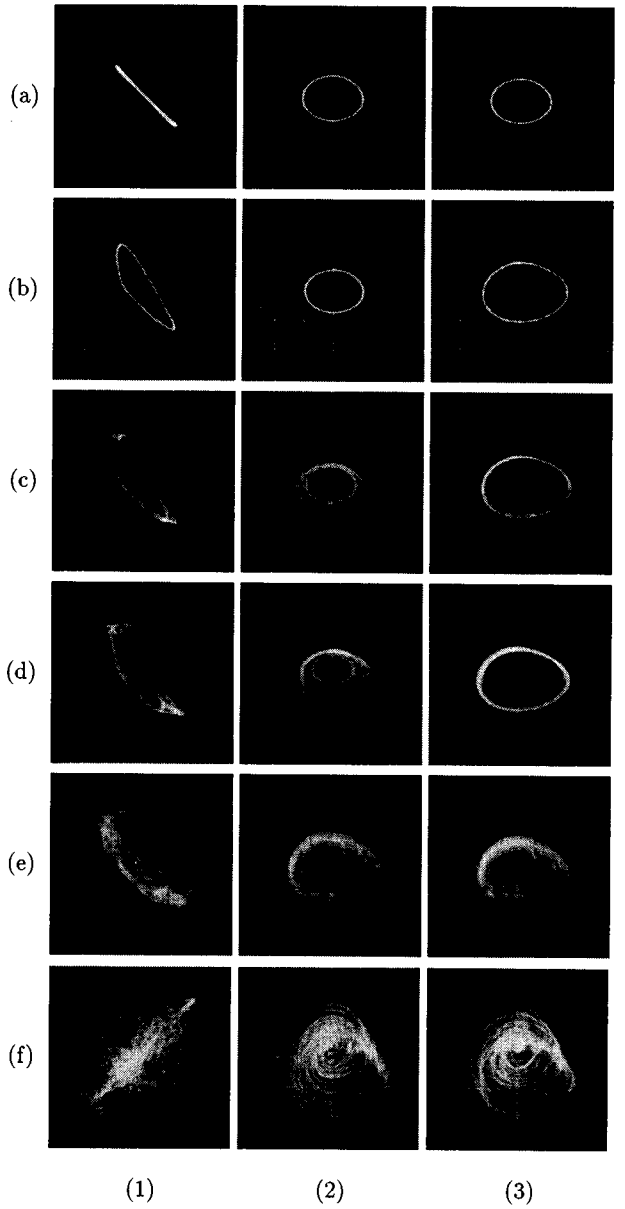

Fig. 9 Anti-phase synchronization (circuit experiment). L_0 = 110.3 mH, L_1 = 57.6 mH ± 0.1%, L_2 = 10.2 mH ± 0.1%, C = 68.3 nF ± 0.1%. (a) r = 5.00 kΩ, (b) r = 2.19 kΩ, (c) r = 2.05 kΩ, (d) r = 1.96 kΩ, (e) r = 1.87 kΩ, (f) r = 1.46 kΩ. (1) v_1 vs. v_2, Horizontal and Vertical: 0.5 V/div, (2) v_1 vs. $i_{L_{11}}$, (3) v_2 vs. $i_{L_{12}}$, Horizontal: 0.5 V/div, Vertical: 0.5 mA/div.

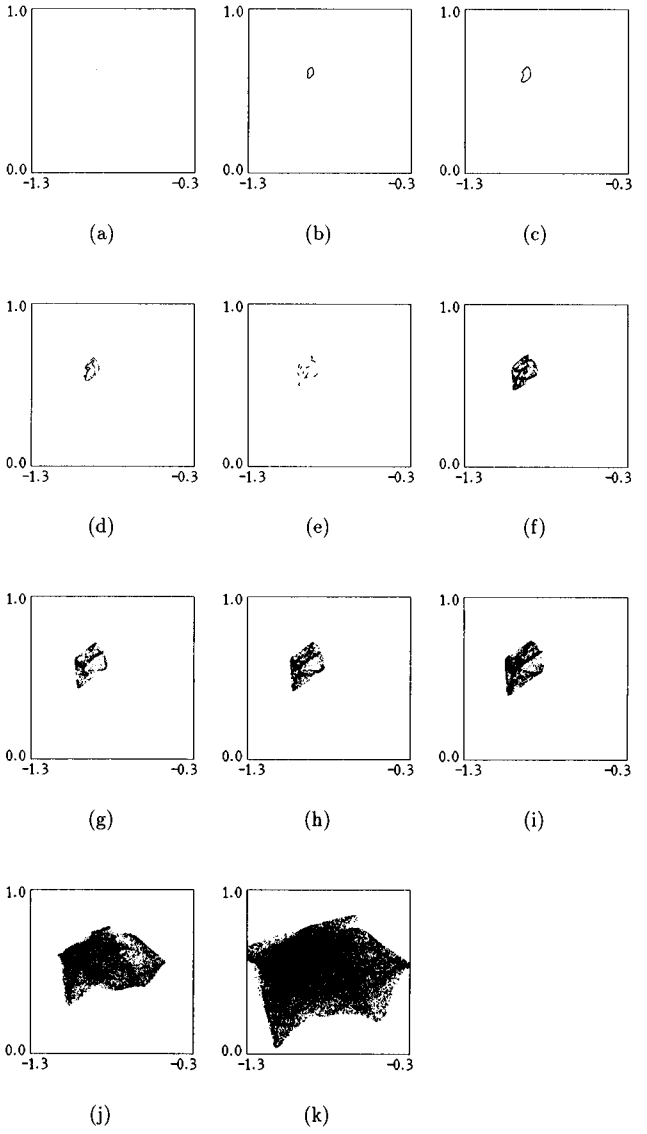

Fig. 10 Poincaré map of anti-phase synchronization. Horizontal: x_1. Vertical: x_2. α = 0.60. β = 6.0. γ : (a) 0.125, (b) 0.140, (c) 0.147, (d) 0.155, (e) 0.160, (f) 0.165, (g) 0.172, (h) 0.175, (i) 0.180, (j) 0.200, (k) 0.235.

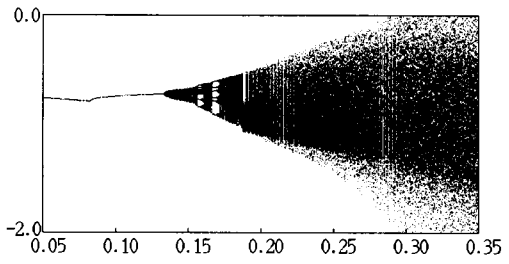

Fig. 11 Bifurcation diagram for the anti-phase synchronization. α = 0.60. Horizontal: γ, Vertical: x_1.

shown in Fig. 12. We can classify characteristics of chaos as follows. The attractors for $0.130 \leqq \gamma \leqq 0.155$ are classified to torus, because the largest Lyapunov exponent λ_1 is equal to 0. While the parameter γ is between 0.160 and 0.165, and larger than 0.170, the attractors are chaos because λ_1 is larger than 0. We can classify that the attractors in Fig. 10 (h) and (i) are area-expanding chaos and that the attractors in Fig. 10 (j) and (k) are volume-expanding chaos. Further, we can also confirm that hyperchaos with three positive Lyapunov exponents exists at $\gamma > 0.260$. Namely, we have found that anti-phase quasi-synchronization bifurcates from one-periodic attractor to hyperchaos with three positive Lyapunov exponents. Furthermore, at

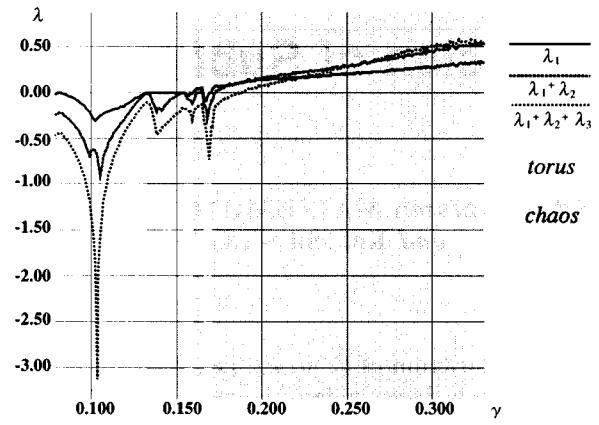

Fig. 12 Lyapunov exponents of the anti-phase synchronization.

$\gamma > 0.320$ we observed self-switching phenomena, however, we found that it has no large extra change.

6. Conclusions

In this paper, we have investigated two types of synchronization modes of in-phase and anti-phase observed from simple chaotic circuits coupled by an inductor. From circuit experiments and computer calculations, we have clarified the bifurcation route of two types of synchronization modes. From Lyapunov exponents calculated by using exact solutions, various bifurcation phenomena have been clarified.

To analyze other coupled systems by using this technique, e.g. two chaotic circuits coupled by a capacitor or some chaotic circuits coupled as a chain, is our future research objective.

Acknowledgment

The authors would like thank to Prof. Toshimichi Saito of Hosei University, for valuable comments and encouragement.

References

[1] Y. Ohmori, M. Nakagawa, and T. Saito, "Mutual coupling of oscillators with chaos and period doubling bifurcation," Proc. of ISCAS'86, pp.61–64, 1986.
[2] L.M. Pecora and T.L. Carroll, "Synchronization in chaotic systems," Phys. Rev. Lett., vol.64, no.4, pp.821–824, 1990.
[3] N. Platt, E.A. Spiebel, and C. Tresser, "On-off intermittency: A mechanism for bursting," Phys. Rev. Lett., vol.70, no.3, pp.279–282, Jan. 1993.
[4] E. Ott and T.C. Sommerer, "Blowout bifurcations: The occurrence of riddled basins and on-off intermittency," Phys. Lett. A, vol.188, pp.39–47, May 1994.
[5] P. Ashwin, J. Buescu, and I. Stewart, "Bubbling of attractors and synchronization of chaotic oscillators," Phys. Lett. A, vol.193, pp.126–139, 1994.
[6] Y. Nishio and A. Ushida, "On a ring of chaotic coupled by inductors," IEICE Trans., vol.E78-A, no.5, May 1995.
[7] T. Yoshinaga, H. Kitajima, and H. Kawakami, "Bifurcation in a coupled Rössler system," IEICE Trans., vol.E78-A, no.10, Oct. 1995.
[8] N. Inaba and S. Mori, "Chaotic phenomena in a circuit with a diode due to the change of the oscillation frequency," IEICE Trans., vol.E71, pp.842–849, Sept. 1988.
[9] N. Inaba and T. Saito, "Chaotic phenomena in a circuit with a negative resistance and an ideal switch of diodes," IEICE Trans., vol.E70, no.8, pp.744–754, Aug. 1987.
[10] T. Saito, "The dead-zone conductor hyperchaos generator," IEICE Trans., vol.J72-A, no.7, pp.1084–1092, July 1989.
[11] Y. Nishio, N. Inaba, and S. Mori, "Chaos in a four-dimensional autonomous circuit with two diodes," Electronics and Communication in Japan, part 3, vol.74, no.11, pp.77–89, 1991.

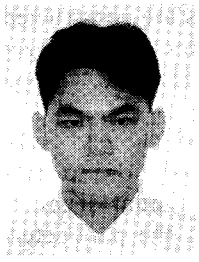

Masahiro Wada was born in Nara, Japan, on 1972. He received the B.E. and M.E. degrees from Tokushima University, Tokushima, Japan, in 1995, 1997, respectively. He is currently working towards Ph.D. degree at the same university. His research interest is in chaos in nonlinear circuits.

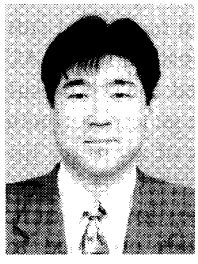

Yoshifumi Nishio received the B.E. and M.E. and Ph.D. degrees in Electrical Engineering from Keio University, Yokohama, Japan, in 1988, 1990 and 1993, respectively. In 1993, he joined the Department of Electrical and Electronic Engineering at Tokushima University, Tokushima Japan, where he is currently an Associate Professor. His research interests are in chaos and synchronization phenomena in nonlinear circuits. Dr. Nishio is a member of the IEEE.

Akio Ushida received the B.E. and M.E. degrees in electrical engineering from Tokushima University in 1961 and 1966, respectively, and the Ph.D. degree in electrical engineering from University of Osaka Prefecture in 1974. He was an associate professor from 1973 to 1980 at Tokushima University. Since 1980 he has been a Professor in the Department of Electrical Engineering at the university. From 1974 to 1975 he spent one year as a visiting scholar at the Department of Electrical Engineering and Computer Sciences at the University of California, Berkeley. His current research interests include numerical methods and computer-aided analysis of nonlinear systems. Dr. Ushida is a member of the IEEE.